A MONTE CARLO STUDY OF INSOLUBLE BLOCK ORIENTATIONS IN SWOLLEN CORES OF MULTIMOLECULAR BLOCK COPOLYMER MICELLES

Zuzana LIMPOUCHOVA and Karel PROCHAZKA

Department of Physical and Macromolecular Chemistry, Charles University, 128 40 Prague 2, The Czech Republic

Received November 8, 1993
Accepted January 3, 1994

Conformations of tethered chains in restricted spherical volumes with an increasing radius were studied by Monte Carlo simulations. Simulations were performed on a tetrahedral lattice at relatively high densities of the occupied lattice sites. A simultaneous self-avoiding walk of all tethered chains creates the starting conformations of the multi-chain system which are futher equilibrated by a modified algorithm similar to that of Siepmann and Frenkel. In this paper, only a geometric excluded volume effect of segments is considered. Selectively chosen series of data for changing numbers of chains, *N*, their lengths, *L*, and radii of the sphere, *R*, give information on the system behavior under various conditions. In this part of our systematic study of tethered chains in constrained volumes, we present angular distribution functions of the end-to-end, end-to-gravity center distances, etc. for system studied in previous paper. The second class of studied conformational characteristics are the distributions of projections of the end-to-end vectors into the selected directions (i.e. the radial direction and the direction of the first-to-second polymer segment connection).

Block copolymers AB, or ABA form in dilute solutions in selective solvents (a good solvent for block A, and a non-solvent for B) multimolecular micelles[1,2]. Polymeric micelles are reversible spherical associates, fairly monodisperse in mass and size. A typical micelle contains several tens to a few hundreds of copolymer chains and is quite small for its high molar mass. It consists of a compact spherical core formed by insoluble blocks (the average segment density 0.7 – 0.8 g cm^{-3}) and a diffuse protective outer shell formed by soluble blocks (segment density ca 0.15 – 0.25 g cm^{-3}). Micellization process resembles in many respects that of soaps and detergents and obeys a model of a closed association[3]: Monodisperse micelles are in a reversible equilibrium with a certain concentration of non-micellized copolymer (unimer) and the association number, *n*, depends on the thermodynamic conditions, but not on the total copolymer concentration. In some systems (e.g. amphiphilic block copolymers in aqueous media) the equilibrium is kinetically frozen and the behavior of the system may differ considerably from the above outlined scheme[4 – 7].

Equilibrium properties of micellizing systems depend both on the state of the core and the shell. In a simple reversible system without any specific interactions, thermodynamics of the core is supposed to play a decisive role in micellization processes in the whole system[8 – 12]. Several thermodynamic theories have been developed for the description of the micellization equilibrium[8 – 15]. All of them had to use rather cruel approximations for various contributions to the Gibbs free energy of the equilibrium system (describing the core, core/shell interface, or shell behavior) and the agreement with existing experimental data in a broad range of experimental conditions is only qualitative.

Great improvements in the understanding of multi-chain systems behavior at elevated segment densities, or in restricted geometries have been achieved in the last few years by computer simulations[16 – 20]. Quite recently, Mattice et al.[21 – 25] were able to simulate a spontaneous micellization of short AB and ABA copolymer chains on a simple cubic lattice without any limiting assumptions on the system behavior. The authors did not study structural details of chain arrangements in micelles since the studied chains were too short.

Conformations of chains tethered to flat, or curved convex surfaces have been studied by several authors[18 – 20]. Behavior of dense multi-chain systems in small closed volumes is a less investigated topic despite its enormous theoretical and practical importance. In the two preceding papers of this series[26,27] we have presented the first simulated data on the chain conformations in small spherical volumes. In this paper we present the angular distributions of chain orientations (e.g. the angular distribution of the tethered end-to-the free end orientations with respect to the radial direction, etc.) for systems which had been studied in previous paper (i.e. for systems that realistically mimic swollen cores of polymeric micelles).

Analogically to our previous studies, only the geometrical excluded volume effect has been taken into consideration. Behavior of systems with the *trans*/*gauche* isomeric states potential and the non-bonding interaction potential is a subject of the ongoing studies. Nevertheless, in the absence of very strong specific interactions, structural properties of dense and constrained systems on a tetrahedral lattice are controlled mainly by the excluded volume effect.

METHOD

The Simulation Procedure

Simulation procedure used in this paper is the same as in our previous studies[26,27]: It consists of: (i) a simultaneous self-avoiding walk of all chains tethered to the surface inside the spherical volume, and (ii) an equilibration algorithm similar to that of Frenkel and Siepmann[16]. Randomly chosen chains are disregarded one by one and they grow again in the dense multi-chain system. The acceptance of a newly grown chain is

subjected to a modified Metropolis criterion[28] for the Rosenbluth weights[29] of the new and the old chain conformations, W_{new}/W_{old}. Only the geometrical excluded volume effect is considered. All details of the simulation procedure have been described in previous parts of this series[26,27]. Individual distributions are based on 10^4 successfully created and statistically non-correlated multi-chain system configurations (i.e. $10^8 - 10^9$ generations of segment positions). Simulations were performed on a DEC 5000/200 computer using an original program in FORTRAN 77. The longest simulations took up to two weeks of the CPU.

Calculated Distribution Functions

The following distribution functions are presented in this communication:

a) The angular distribution of directions of the tethered end-to-the free chain end with respect to the radial direction, $\Psi_{TF}^{(r)}(\vartheta)$. This function is constructed as a histogram during simulations of individual multi-chain configurations (see ref.[26]). Its values are normalized by numbers of all lattice sites in volume elements confined between two cones with the common apex at the surface (an inner cone with the angle ϑ, and the outer with $\vartheta + \Delta\vartheta$, $\Delta\vartheta = 5°$) – see Fig. 1*a*. Those normalization numbers are averaged over all lattice sites in the surface layer of the thickness $\Delta = 0.1\ l$ (the possible apex locations). Function $\Psi_{TF}^{(r)}(\vartheta)$ is a mean angular distribution function, averaged over all possible end-to-end distances, r_{TF} (it depends on ϑ, but not on r_{TF}). The correlated distribution functions, $P_{TF}^{(r)}(r_{TF}, \vartheta)$, as functions of both the distances r_{TF} and orientations ϑ with respect to the radial direction will be presented in our next publication[30]. A similar function to $\Psi_{TF}^{(r)}(\vartheta)$ is the angular distribution of the tethered end-to-the center of gravity orientation with respect to the radial direction, $\Psi_{TC}^{(r)}(\vartheta)$.

Three other angular functions (with respect to the radial direction) were calculated in the course of computer simulations: The average number fraction of chains with certain end-to-end, or end-to-center of gravity orientations, $n_{TF}^{(r)}(\vartheta)$, $n_{TC}^{(r)}(\vartheta)$, and $n_{FC}^{(r)}(\vartheta)$, respectively. The first and the second functions are recalculable from corresponding normalized functions, $\Psi_{TF}^{(r)}(\vartheta)$ and $\Psi_{TC}^{(r)}(\vartheta)$, nevertheless the possibility to compare both types of curves helps to the reader to assess the significance of an orientation effect of the external constraints. In the last case, the "normalization cones" depend on positions of free ends and the centers of gravity of individual chains in the sphere and the physical significance of the normalization procedure is not clear. It is the reason why we present only the function $n_{FC}^{(r)}(\vartheta)$.

b) Angular distribution functions with respect to the direction of the first-the second segment connection (characterized by an angle φ): The number fraction of chains as a function of orientations of the end-to-end vectors, $n_{TF}^{(12)}(\varphi)$, see Fig. 1b.

Further calculated functions are distributions (number fractions) of projections of the end-to-end, or end-to-the center of gravity distances into:

c) the radial direction, $f_{TF}^{(r)}(p_{TF}^{(r)})$, $f_{TC}^{(r)}(p_{TC}^{(r)})$ and $f_{FC}^{(r)}(p_{FC}^{(r)})$ respectively, or

d) into the direction of the first-the second segment connection, $f_{TF}^{(12)}$ ($p_{TF}^{(12)}$) (see Fig. 2).

RESULTS AND DISCUSSION

Orientational Distribution Functions with Respect to the Radial Direction

Figure 3 shows the normalized angular distribution function of orientations of end-to-end distances with respect to the radial direction, $\Psi_{TF}^{(r)}(J)$, for multi-chain systems (mod-

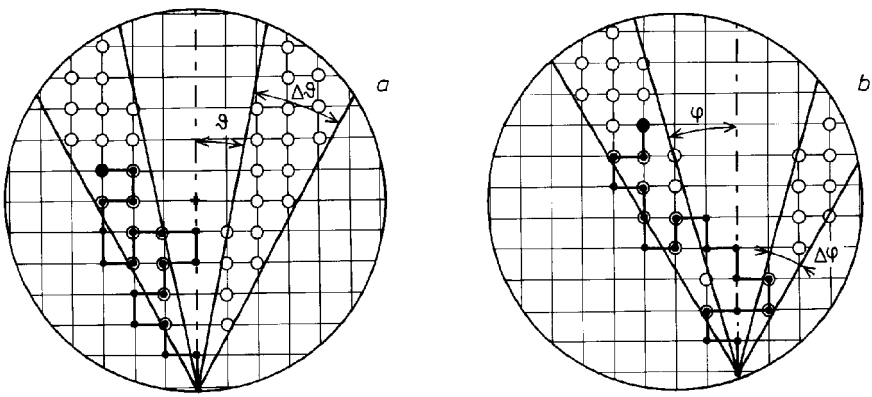

FIG. 1
A schematic two-dimensional representation of the evaluation of: *a* angular distribution function with respect to the radial direction, $\Psi_{TF}^{(r)}(J)$; *b* an analogical function with respect to the direction of the first-to-second segment connection, $\Psi_{TF}^{(12)}(j)$; the real angular intervals used in calculations are: $\Delta\vartheta = 5°$, $\Delta\varphi = 5°$

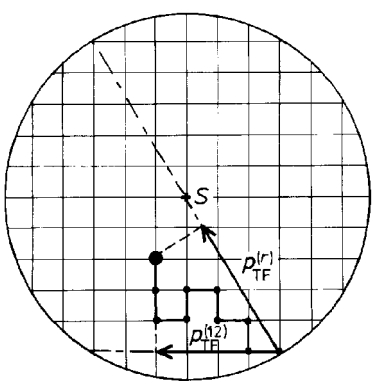

FIG. 2
A schematic two-dimensional representation of the evaluation of projections of the end-to-end connection into the radial direction, $p_{TF}^{(r)}$, and into the direction of the first-to-second segment connection, $p_{TF}^{(12)}$

elling moderately swollen micellar cores) for three radii of the sphere, R = 10 l, 12.5 l and 15 l (l is the lattice distance), a constant average segment density $\langle g_S \rangle = (N L/N_{tot}) = 0.52$, and various numbers N and L, $N \in \langle 15, 86 \rangle$, $L \in \langle 33, 163 \rangle$.

General shape of all curves is basically the same with a relatively broad and deep minimum in the region ϑ = 0 to 45° and a pronounced maximum around ϑ = 65 to 70°. At higher angles, the curves drop again and their values close to ϑ = 90° correspond roughly to those for ϑ = 0°. Shapes with well-pronounced maxima are typical for small

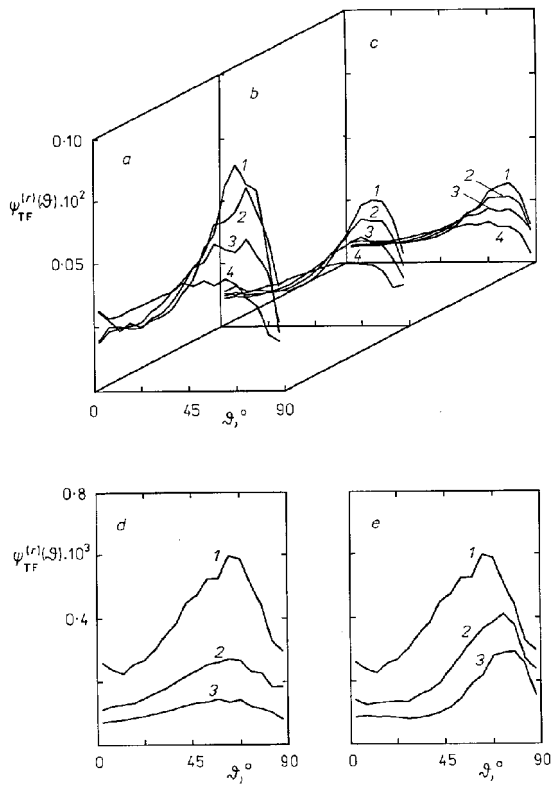

FIG. 3

Angular distribution functions of orientations of the tethered-to-free end connections of individual chains with respect to the radial direction in spherical micellar cores, $\Psi_{TF}^{(r)}(J)$, for two constant segment densities: $\langle g_S \rangle$ = 0.52 (*a, b, c*) and $\langle g_S \rangle$ = 0.36 (*d, e*). Values of the other parameters: *a*: R = 10 l, N/L = 45/31 (*1*), 35/40 (*2*), 25/56 (*3*) and 15/93 (*4*); *b*: R = 12.5 l, N/L = 68/40 (*1*), 53/52 (*2*), 38/72 (*3*) and 23/119 (*4*); *c*: R = 15 l, N/L = 86/55 (*1*), 67/71 (*2*), 48/99 (*3*) and 29/163 (*4*); *d*: a constant number of chains, N = 21 and L = 47, R = 10 l (*1*), L = 92, R = 12.5 l (*2*) and L = 159, R = 15 l (*3*); *e*: a constant chain length, L = 47 and N = 21, R = 10 l (*1*), N = 41, R = 12.5 l (*2*) and N= 71, R = 15 l (*3*)

spheres and high numbers of chains, *N*. In those cases, the maximum values are ca three times higher than the values for $\vartheta = 0°$.

The shape of curves $\Psi_{TF}^{(r)}(J)$ with highly pronounced maxima for angles differing significantly from $\vartheta = 0°$, which suggest a high fraction of "oblique chain orientations" in spherical cores, are slightly surprising. It is quite understandable that not all chain free ends may be located in a small central region of the sphere. The higher is the number of chains, the higher fraction of the free ends is forced to be placed outside the central region. Functions $\Psi_{TF}^{(r)}(J)$ are normalized by numbers of all lattice sites in directions defined by cones with angles ϑ and $(\vartheta + \Delta\vartheta)$ – see Fig. 1, and are therefore corrected for the effect of the changing numbers of lattice sites for a possible location of the chain free ends in individual conical layers. On the basis of pure geometric considerations, one would expect rather broad and flat distributions of chain free end orientations into all possible angles ϑ, <0, 90°>, without any token of a minimum close to $\vartheta = 0°$. The surprising shape with the pronounced maximum for non-zero angles is mainly a consequence of the general behavior of a single chain in a restricted volume[30] (see the summarizing discussion concerning Figs 3 – 7).

Conclusions which may be drawn from the simulated angular distributions agree with the indirect observations made in our previous papers[26,27]. On the basis of a comparison of the distribution of the end-to-end distances, $\rho_{TF}(r_{TF})$, with the distribution of the free end locations within the sphere, $g_F(r)$, we have suggested earlier that a nonnegligible fraction of chains decline appreciably from the radial direction.

Figure 3*d* shows three curves $\Psi_{TF}^{(r)}(J)$ for a constant segment density, $\langle g_S \rangle = 0.36$, a constant number of chains, $N = 21$, and increasing lengths of chains which is proportional to R^3. Numbers of lattice sites for a location of any segment in all $\Delta\vartheta$ intervals increase with increasing R and it results in flat functions $\Psi_{TF}^{(r)}(J)$ for the largest $R = 15\ l$.

An interesting trend may be observed in Fig. 3*e*. The curves for chains of the same length, $L = 47$, show slightly different angular orientations in volumes with the increasing R. An evident shift in the maxima positions with the increasing R may be observed. This confirms our earlier indirect conclusion which we had made in our previous study on the basis of the comparison of the function $\rho_{TF}(r_{TF})$, with the distribution of the free end locations in the sphere, $g_F(r)$, for a constant L – see Figs 1*e* and 4*e* in ref.[27].

Figure 4 gives a supplementary information on the number fraction of chains with particularly oriented end-to-end connections, $n_{TF}^{(r)}(\vartheta)$. Functions $\Psi_{TF}^{(r)}(J)$ and $n_{TF}^{(r)}(\vartheta)$ are recalculable from each other on the basis of our calculation procedure, nevertheless it would be very difficult for a reader to deduce the correct shape of the latter distribution from the first one without other information. A relatively high maximum in the number of chains is achieved for orientations between $\vartheta = 30 - 50°$ for all systems. All curves go almost to zero for $\vartheta = 0°$ due to a very small number of lattice sites in a narrow cone with the apex angle $\Delta\vartheta = 10°$.

Distribution functions of the tethered end-to-center of gravity orientations, $\Psi_{TC}^{(r)}(J)$, are shown in Fig. 5. All curves $\Psi_{TC}^{(r)}(J)$ have a broad minimum for angles $\vartheta = 0 - 25°$. Then they rise steeply and reach a sharp maximum around $\vartheta = 45 - 55°$ and drop suddenly to zero for angles $\vartheta > 50 - 60°$. Positions of the maximum, as well as the position of the sudden drop depend sensitively on N, but they do not depend on L (see Fig. 5*d*, *e*). The shape with a well-pronounced maximum is typical for systems with small R and it does not nearly depend on the average segment density, $\langle g_S \rangle$. Position of the maximum (the angle ϑ_m) increases with the increasing number of chains, N. It is interesting to compare distribution functions, $\Psi_{TC}^{(r)}(J)$, with corresponding functions, $\Psi_{TF}^{(r)}(J)$. Shapes of $\Psi_{TC}^{(r)}(J)$ suggest a narrower angular distribution of the "tethered halves" of chains in comparison with the "whole chain orientations".

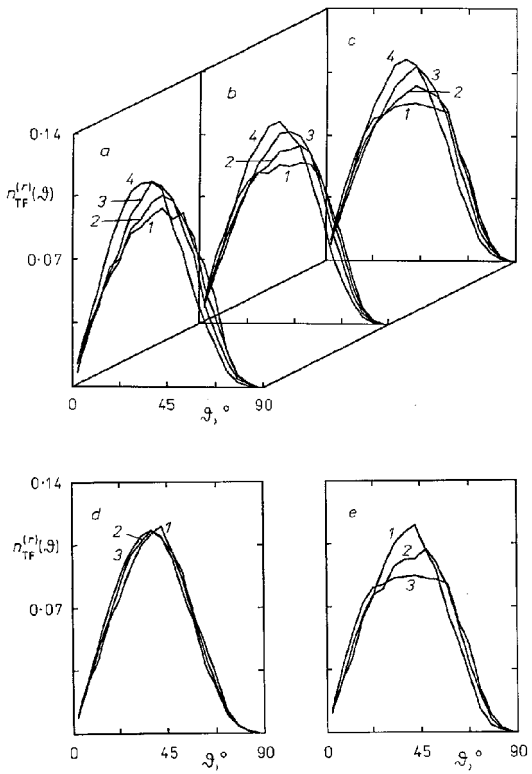

FIG. 4
Number fractions, $n_{TF}^{(r)}(\vartheta)$, of chains with given end-to-end orientations corresponding to distribution functions in Fig. 3

Figure 6 shows the number fractions, $n_{TC}^{(r)}(\vartheta)$, of chains corresponding to functions $\Psi_{TC}^{(r)}(J)$. A significant maximum between 30 and 50° is attained for all systems. The main difference between $n_{TF}^{(r)}(\vartheta)$ and $n_{TC}^{(r)}(\vartheta)$ consists in the fact that the latter falls fast to zero for $\vartheta = 70 - 90°$.

The effect of *R*-dependent geometrical constrains on the angular distributions, $\Psi_{TF}^{(r)}(J)$ and $\Psi_{TC}^{(r)}(J)$, is quite important as compared with distribution functions of distances, $\rho_{TF}(r_{TF})$, $\rho_{TC}(r_{TC})$, etc. which were presented earlier[26,27].

Figure 7 shows the number fractions of chains with given angular orientations of the free end-to-center of gravity connections, $n_{FC}^{(r)}(\vartheta)$. For the physical and computational reasons discussed in the methodological section, we present only $n_{FC}^{(r)}(\vartheta)$, and not the function $\Psi_{FC}^{(r)}(J)$. Simulated curves show broad distributions of the considered connections into all possible directions (in the whole angular range, $\vartheta = 0$ to 180°) with a

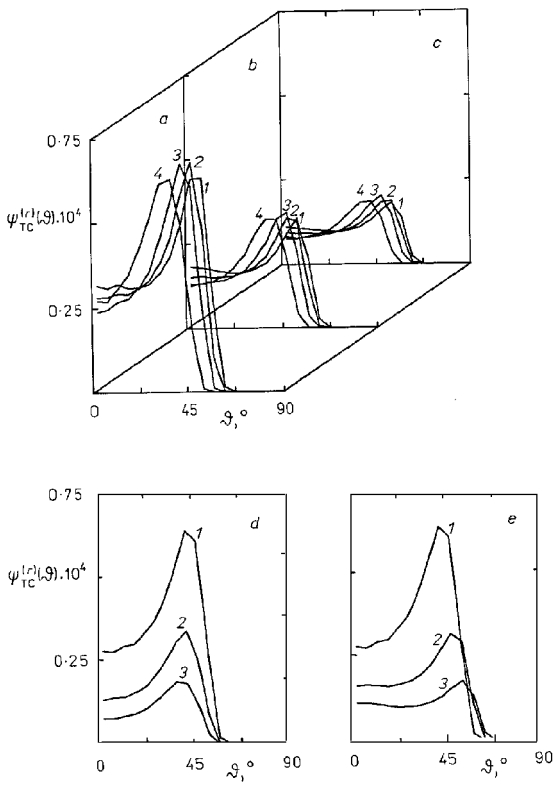

FIG. 5
Angular distribution function of the tethered end-to-the gravity center orientations with respect to the radial direction, $\Psi_{TC}^{(r)}(J)$, for the same systems as in Fig. 3

significant maximum slightly below $\vartheta = 90°$ which means that the highest fraction of the free end-to-gravity center connections are oriented almost perpendicularly to the radial direction.

It may be summarized on the basis of Figs 3 – 7 that the "tethered halves" of chains are more affected by the strongly curved surface and are therefore more radially oriented than the "free halves". This result agrees with what may be expected for such systems. An interesting effect, which is not easy to account for by simplified geometric considerations, is demonstrated by an increased fraction of chains in the distribution function, $\Psi_{TC}^{(r)}(J)$, in a strikingly narrow angular range between 40 and 55° and almost zero fractions, $\Psi_{TC}^{(r)}(J) = 0$, for $\vartheta > 60°$. This behavior may be traced upto very low segment densities (it is evident even in a system consisting of one moderately long tethered chain, i.e. $L < 5\ R/l$, in otherwise empty spherical core). This is probably

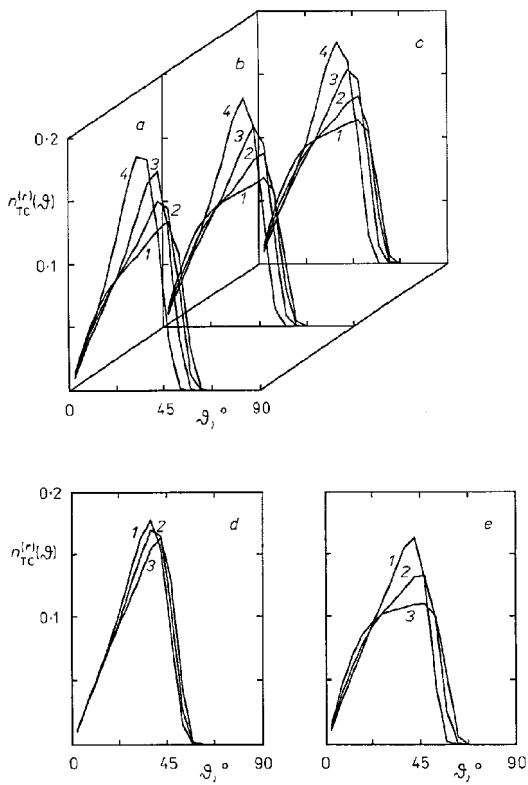

FIG. 6
Number fractions, $n_{TC}^{(r)}(\vartheta)$, of chains with given tethered end-to-the gravity center orientations corresponding to distribution functions in Fig. 5

caused by the maximum entropy principle in a very constrained volume (an optimum utilization of the entire volume by moderately stiff chains) together with an orientational effect of the curved surface on the tethered part of a chain[30].

Distributions of Various Projections into the Radial Direction

Figures 8 and 9 show the distribution functions of projections of the end-to-end distances and the tethered end-to-the center of gravity distances into the radial direction, $f_{TF}^{(r)}(p_{TF}^{(r)})$ and $f_{TC}^{(r)}(p_{TC}^{(r)})$, respectively. The shape and particularly the broadness of the curves reflect to a high degree the flexibility of chains in the dense system under given conditions (i.e. under given geometrical constraints) and the loss of memory concerning the orientational effect of the strongly curved surface in the succession of segments (from the tethered end upto the free end, or upto the gravity center). Distributions for

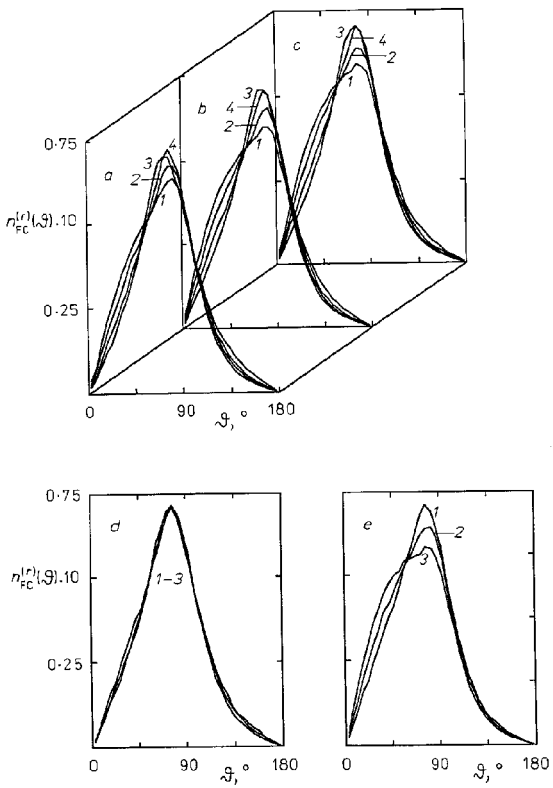

FIG. 7
Number fractions, $n_{FC}^{(r)}(\vartheta)$, of chains with given free end-to-the gravity center orientations

shorter chains are much narrower than those for long chains and that indicates a considerable orientational effect within the whole chain which is transmitted from segment to segment due to a reduced flexibility of short chains in constrained systems. Curves in Figs 8*e* and 9*e* confirm the interesting feature of the behavior of the studied systems that we have found earlier[26,27]: The geometrical constraints, even though very important and predetermining to a great extent the general properties of the system, do not change fast in the region of $R \in \langle 10\,l, 15\,l \rangle$ and the functions describing properties of individual chains at a constant average segment density, $\langle g_S \rangle$, depend mainly on the chain length, L, (see also Figs 8*d* and 9*d*) and depend only little on N and R.

Figure 10 shows distribution functions of projections of the free end-to-the center of gravity distances into the radial direction, $f_{FC}^{(r)}(p_{FC}^{(r)})$. As concerns those projections, they may be oriented both in the positive (central) and negative (centrifugal) directions.

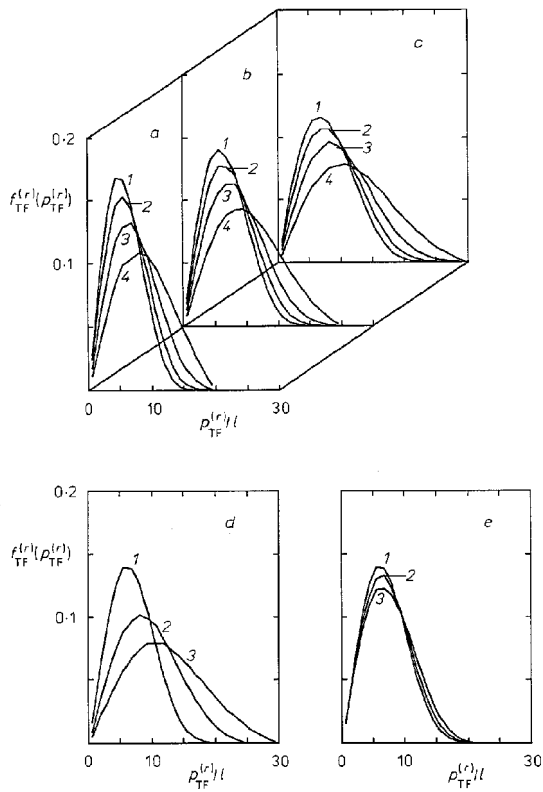

FIG. 8
Distribution function of projections of the tethered end-to-free end distances into the radial direction, $f_{TF}^{(r)}(p_{TF}^{(r)})$, for the same systems as in Fig. 3

Distributions $f_{FC}^{(r)}$ ($p_{FC}^{(r)}$) reach their maxima for positive values, p_{FC} ca 2.5 l – 3 l, and their shapes suggest that only a smaller fraction of "chain free halves" coil back to the surface of the sphere. This behavior of "free halves" was found almost identical for all studied systems.

Persistence Characteristics

To complete the characterization of the conformational behavior of individual chains in constrained spherical volumes, we present angular distributions of chain end-to-end distances with respect to the orientation of the first-to-second segment connection, $n_{TF}^{(12)}(\varphi)$, and distributions of projections of the end-to-end distances into the direction of the first-to-second segment connection, $f_{TF}^{(12)}$ ($p_{TF}^{(12)}$). These functions reflect to a certain degree the "memory of the chain" concerning the direction of its very beginning and

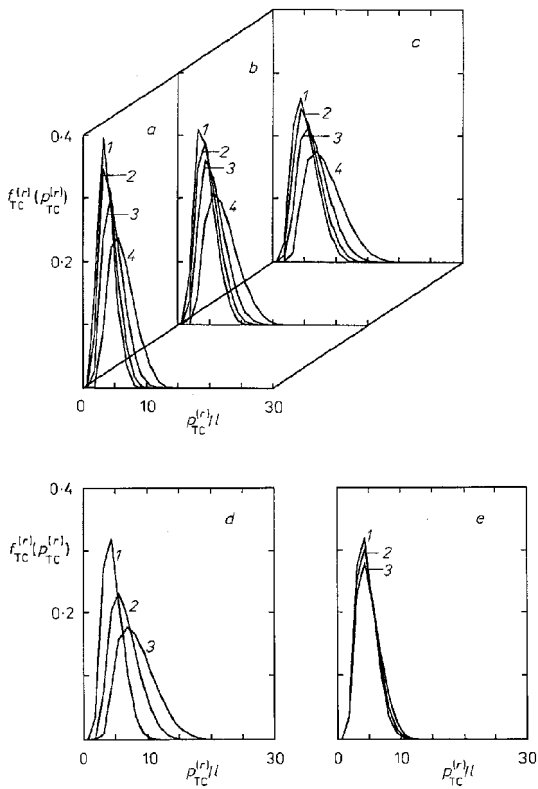

FIG. 9
Distribution function of projections of the tethered end-to-the gravity center distances into the radial direction, $f_{TC}^{(r)}$ ($p_{TC}^{(r)}$), for the same systems as in Fig. 3

reflect thus the effective stifness of the chain under given conditions, nevertheless they are not directly affected by the orientational effect of the curved surface.

Figure 11 shows the angular distribution functions (i.e. the number fractions), $n_{TF}^{(12)}(\varphi)$. Curves for all systems are identical within the range of error of statistical Monte Carlo simulations. Low values of $n_{TF}^{(12)}(\varphi)$ for $\varphi \to 0$ are caused by a small number of lattice sites in a cone with a small apex angle $\Delta\varphi = 10°$. Maxima are reached close to $\varphi = 60°$. Simulated curves are quite asymmetrical with pronounced tails for higher angles φ, nevertheless the fractions of chains for $\varphi > 135°$ are almost negligible.

Distribution functions of projections of the end-to-end distances into the direction of the first-to-second segment connection, $f_{TF}^{(12)}(p_{TF}^{(12)})$, are given in Fig. 12. Functions are almost symmetrical with maximum at ca $p_{TF}^{(12)} = 6\ l$ (this value is close to the average value, $\langle p_{TF}^{(12)} \rangle$, i.e. to the persistence length). It is certainly interesting to compare dis-

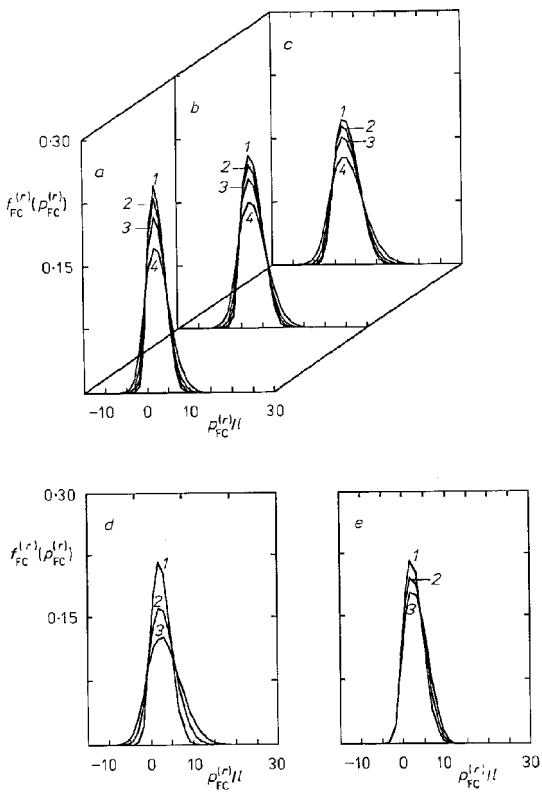

FIG. 10
Distribution function of projections of the free end-to-the gravity center distances into the radial direction, $f_{FC}^{(r)}(p_{FC}^{(r)})$, for the same systems as in Fig. 3

tribution function, $f_{TF}^{(12)}(p_{TF}^{(12)})$, with the analogical function, $f_{TF}^{(r)}(p_{TF}^{(r)})$. The latter function is defined only for positive values of $p_{TF}^{(r)}$, is quite asymmetrical and the maximum position depends significantly on the chain length, L. The first one is non-zero for negative $p_{TF}^{(12)}$, and is almost symmetrical with respect to the maximum position which does not nearly depend on L. We may conclude that a certain residual and slowly decaying information on the orientation of the first-to-second segment connection is carried out, conserved and "complied" throughout the full succession of segments in the chain. We would like to stress that those persistence properties of individual chains are affected by complicated behavior of the whole system and that they reflect the effective stiffness of chains in severly constrained systems.

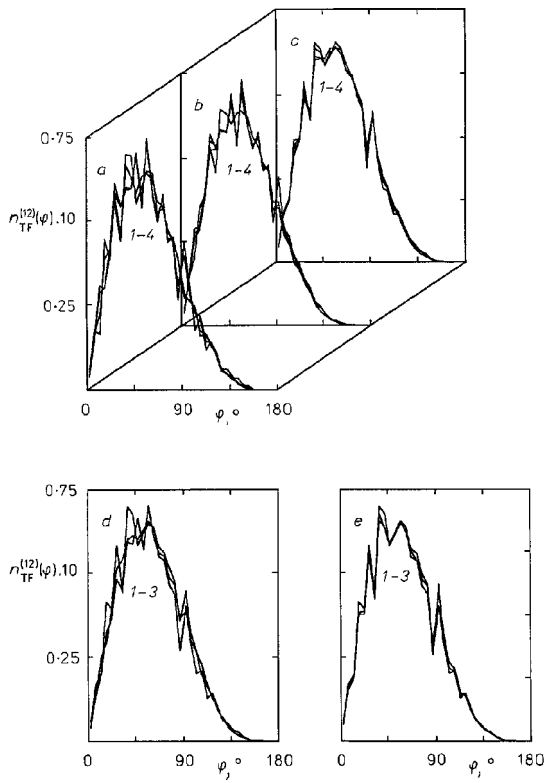

FIG. 11

Number fractions, $n_{TF}^{(12)}(\varphi)$, of chains with given end-to-end orientations with respect to the direction of the first-to-second segment connection for the same systems as in Fig. 3

CONCLUSIONS

a) Results of the performed Monte Carlo simulations presented in this paper broaden the knowledge of the conformational behavior of tethered chains in constrained concave volumes: The multi-chain system is fairly disordered and a significant fraction of chains declines to a certain degree from the radial direction.

b) Distributions of the projections of the free end-to-the gravity center connections into the radial direction, $f_{FC}^{(r)}(p_{FC}^{(r)})$, suggest that a non-negligible fraction of chain "free halves" are oriented back towards the surface of the sphere.

c) A great majority of conformational characteristics of individual tethered chains depend only little on the average segment densities in the sphere. Some of them are qualitatively the same for constrained multi-chain systems and for an "isolated" tethered chain submitted to identical constraints (i.e. in otherwise empty sphere). It may

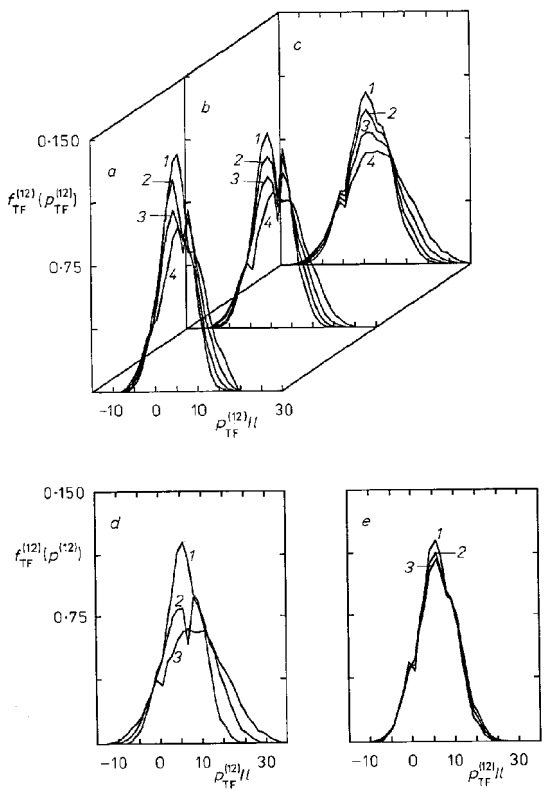

FIG. 12
Distribution function of projections of the tethered end-to-free end distances into the direction of the first-to-second segment connection, $f_{TF}^{(12)}(p_{TF}^{(12)})$, for the same systems as in Fig. 3

be deduced that in the region of the studied segment densities (upto ca 0.5), the inter-chain conformational correlations play a less important role than it may be expected.

The authors are obliged to Prof. P. Munk from the University of Texas at Austin, U.S.A., for helpful discussions and suggestions. The authors thank to the Ministry of Education of the Czech Republic for the financial support of this work (Grant No. FDR 0145) and to the Grant Agency of the Czech Republic (Grant No. 203/93/2287).

REFERENCES

1. Tuzar Z., Kratochvil P. in: *Surface and Colloid Science* (E. Matijevic, Ed.), Vol. 15, p. 1. Plenum Press, New York 1993.
2. Riess G., Huertez G., Bahadur P. in: *Encyclopedia of Polymer Sciences and Engineering* (H. Mark, N. M. Bikales, C. G. Overberger and G. Menges, Eds), Vol. 2, 2nd ed., p. 324. Wiley, New York 1985.
3. Ellias H.-G., Barrais R.: Chimia *21*, 53 (1967).
4. Tuzar Z., Webber S. E., Ramireddy C., Munk P.: Polym. Prepr. *32*(1), 525 (1991).
5. Prochazka K., Kiserow D., Ramireddy C., Webber S. E., Munk P., Tuzar Z.: Makromol. Chem., Macromol. Symp. *58*, 201 (1992).
6. Prochazka K., Kiserow D., Ramireddy C., Tuzar Z., Munk P., Webber S. E.: Macromolecules *25*, 454 (1992).
7. Kiserow D., Prochazka K., Ramireddy C., Tuzar Z., Munk P., Webber S. E.: Macromolecules *25*, 461 (1992).
8. de Gennes P. G. in: *Solid State Physics* (J. Liebert, Ed.), Suppl. 14, p. 1. Academic Press, New York 1978; de Gennes G. P.: *Scaling Concepts in Polymer Physics*. Cornell University, Ithaca 1979.
9. Leibler L., Orland H., Wheeler J. C.: J. Chem. Phys. *79*, 3550 (1983).
10. Noolandi J., Hong M. H.: Macromolecules *16*, 1443 (1983).
11. Whitmore D., Noolandi J.: Macromolecules *18*, 657 (1985).
12. Meier D. J.: J. Polym. Sci., C *26*, 81 (1969).
13. Helfland E., Tagami Y.: J. Polym. Sci., B *9*, 741 (1971).
14. Helfland E., Sapse A. M.: J. Chem. Phys. *62*, 1327 (1975).
15. Nagarajan R., Ganesh K.: J. Chem. Phys. *90*, 5843 (1989).
16. Kremer K., Binder K.: Comp. Phys. Rep. *7*, 259 (1988).
17. Allen M. P., Tildesley D. J.: *Computer Simulations of Liquids*. Clarendon Press, London 1986.
18. Murat M., Grest G. S.: Macromolecules *24*, 704 (1991).
19. Kremer K., Grest G. S.: J. Chem. Soc., Faraday Trans. *88*, 1707 (1992).
20. Grest G. S., Murat M. in: *Monte Carlo and Molecular Dynamic Simulations in Polymer Science* (K. Binder, Ed.), in press.
21. Rodrigues K., Mattice W. L.: Polym. Bull. (Berlin) *25*, 239 (1991).
22. Rodrigues K., Mattice W. L.: J. Chem. Phys. *94*, 761 (1991).
23. Rodrigues K., Mattice W. L.: Langmuir *8*, 456 (1992).
24. Wang Y., Mattice W. L., Napper D. H.: Macromolecules *25*, 4073 (1992).
25. Wang Y., Mattice W. L., Napper D. H.: Langmuir *9*, 66 (1993).
26. Limpouchova Z., Prochazka K.: Collect. Czech. Chem. Commun. *58*, 2290 (1993).
27. Prochazka K., Limpouchova Z.: Collect. Czech. Chem. Commun. *59*, 782 (1994).

28. Metropolis N., Rosenbluth A. W., Rosenbluth M. N., Teller A., Teller H.: J. Chem. Phys. *21*, 1087 (1953).
29. Rosenbluth M. N., Rosenbluth A. W.: J. Chem. Phys. *23*, 356 (1955).
30. Prochazka K., Limpouchova Z.: Unpublished results.

Translated by the author (K. P.).